Green Corrosion Inhibition and Adsorption Mechanism of *Ricinus communis L.*Extracts on Mild Steel

Gayatri Maiya Koju[1,2], Anju Kumari Das[3], Dipak Kumar Gupta[1]*, Nabin Karki[2]*, Amar Prasad Yadav[1,a]*

[1]*Central Department of Chemistry, Tribhuvan University, Kathmandu 44613, Nepal*

[2]*Bhaktapur Multiple Campus, Tribhuvan University, Bhaktapur 44800, Nepal*

[3]*Amrit Science Campus, Tribhuvan University, Kathmandu 44600, Nepal*

[a] *Currently @Rajarshi Janak University (RJU), Janakpur, Nepal*

**Authors to whom correspondence should be addressed:*

[1]*Central Department of Chemistry*
Tribhuvan University, 44613 Kathmandu
Nepal

Email: deepakguptas2012@yahoo.com
ORCID ID: https://orcid.org/0000-0001-6010-9495

[2]*Bhaktapur Multiple Campus*
Tribhuvan University, 44800 Bhaktapur
Nepal

Email: nabin.karki@bkmc.tu.edu.np
ORCID ID: https://orcid.org/0000-0003-3858-776X

[1,a]*Amrit Science Campus*
Tribhuvan University, 44600 Kathmandu
Nepal

Email: amar2y@yahoo.com
ORCID ID: https://orcid.org/0000-0002-8592-4856

This article has been accepted for publication and undergone full peer review but has not been through the copyediting, typesetting, and proofreading process, which may lead to differences between this version and the official version of record.

Please cite this article as: Koju G.M., Das A.K., Gupta D.K., Karki N., Yadav A.P. Green Corrosion Inhibition and Adsorption Mechanism of *Ricinus communis L.*Extracts on Mild Steel. *Mongolian Journal of Chemistry*, 27(56), 2026, xx-xx

https://doi.org/10.5564/mjc.v27i56.4946

Green Corrosion Inhibition and Adsorption Mechanism of *Ricinus communis L.*Extracts on Mild Steel

Gayatri Maiya Koju[1,2], https://orcid.org/0000-0002-7491-0731
Anju Kumari Das[3], https://orcid.org/0009-0006-0935-5838
Dipak Kumar Gupta[1]*, https://orcid.org/0000-0001-6010-9495
Nabin Karki[2]*, https://orcid.org/0000-0003-3858-776X
Amar Prasad Yadav[1a]*, https://orcid.org/0000-0002-8592-4856

[1]*Central Department of Chemistry, Tribhuvan University, Kathmandu 44613, Nepal*
[2]*Bhaktapur Multiple Campus, Tribhuvan University, Bhaktapur 44800, Nepal*
[3]*Amrit Science Campus, Tribhuvan University, Kathmandu 44600, Nepal*
[a] *Currently @Rajarshi Janak University (RJU), Janakpur, Nepal*

ABSTRACT

Plant-based corrosion inhibitors offer effective corrosion protection, are eco-friendly and safe, biodegradable, low-cost, readily available, and renewable resources, thereby reducing dependence on chemical-based alternatives. Investigating *Ricinus communis L.* aqueous extracts as corrosion inhibitors for mild steel in an acidic medium is a significant step toward greater efficiency in corrosion research. The corrosion-inhibition behavior of the extracts was studied using the gravimetric method and electrochemical methods. UV-visible spectroscopy, Fourier transform infrared spectroscopy, and gas chromatography–mass spectrometry were used to analyze the extract. Field-emission scanning electron microscopy, atomic force microscopy, and X-ray photoelectron spectroscopy were used to investigate the surface morphology and the protective film. The results suggest that the extracts contain O–H, C–N, and C=C functional groups. These groups play a key role in their corrosion-inhibiting behavior. In an acidic medium, inhibition efficiency increased with increasing extract concentration and decreased with increasing temperature. The inhibition efficiency was maximum at 3 hours, increased with increasing inhibitor concentration, and decreased with increasing temperature. The adsorption isotherm follows Langmuir adsorption, and the thermodynamic parameters indicate that the adsorption follows a mixed-type isotherm. Field emission scanning electron microscopy and atomic force microscopy reveal the adsorption of the extract molecules, showing a smooth surface on the inhibited mild steel. X-ray photoelectron spectroscopy supports the formation of C 1s, O 1s, and N 1s of the extract bonding with Fe 2p on the mild steel in the inhibited sample.

Keywords: *Ricinus communis L.*, Green Inhibitor, Adsorption, Atomic Force Microscopy, X-ray Photoelectron Spectroscopy

INTRODUCTION

Mild steel is very crucial to everyday life because it is one of the strongest, cheapest, and most valuable materials that human beings have invented. Without steel, it would not be possible to lead a modern life. The global demand for the crucial metal is likely to continue rising during the 21st century, with demand projected to increase by 2 to 6 times, depending on the metal [1, 2]. Mild steel is commonly used in industries such as petrochemicals, petroleum, and nuclear due to its good mechanical properties and low production cost. While there are many advantages to using mild steel, a major drawback is its high susceptibility to corrosion, especially in acidic environments [3, 4]. Many economic losses are due to unwanted corrosion of mild steel in acidic media. Further, acidic media are widely used in processes such as rust and scale elimination in acid pickling, boiler scaling, oil well acidization, and other petrochemical applications [5]. While keeping metallic structures safe from acidic environments is the best way to prevent corrosion, it is difficult to achieve. However, several approaches are being used to resist corrosion, including coating protection, alloying, galvanization, and cathodic protection. Among these approaches, corrosion inhibitors can be a very inexpensive and effective way to protect metal surfaces [6]. Corrosion inhibitors are generally classified into two main categories: natural inhibitors and synthetic inhibitors. Natural inhibitors are known to be eco-friendly, biodegradable, and non-toxic because they are obtained from plant extracts and minerals. They can serve as a more environmentally friendly substitute for synthetic inhibitors [4]. In comparison, synthetic inhibitors are chemically manufactured to provide a high degree of protection under a wide range of corrosive conditions. The predominant inhibitors are organic compounds containing heteroatoms and multiple bonds, specifically double or triple bonds. These functional groups serve as primary adsorbent centers owing to their elevated electron density and donating characteristics [4]. It noted that the manufacture and utilization of synthetic organic inhibitors can cause environmental and economic issues regarding their toxicity and the cost of production [7].

Natural products, including plant extracts, are emerging as promising candidates considering their intrinsic biodegradability, non-toxicity, and easy availability. Various literature reports indicate that organic compounds of plant origin, including alkaloids, flavonoids, polyphenols, terpenoids, and carbohydrates, possess molecular and electronic characteristics that are comparable to those of synthetic inhibitors. The inhibition of metal corrosion by plant extracts has been extensively documented in several research works. A few of them are *Hunteria umbellata* Seed Husk extracts [3], *Acalypha chamaedrifolia* leaves

extract [8], *Calotropis Procera* extract [9], Amazonian tree alkaloids extract [10], *Allium sativum* extract [11], acidic extract of bark of *Eucalyptus globules* [12], *Jatropha Curcas* extract [13], Coconut leaf extract [14], methanol extract of *Equisetum hyemale* [15], *Prunus dulcis* leaf extract [16], extract of *Artemisia vulgaris* [17], *Abelmoschus esculentus* and *Citrus maxima* leaf extracts [4] etc.

The scientific name of the castor oil bean plant is *Ricinus communis* L. The castor oil bean plant belongs to the genus Euphorbiaceae. It grows abundantly in the tropics and the subtropics and is one of the most widely grown plants in the world. The plant *Ricinus communis* has been documented to exhibit a diverse array of pharmacological activities, encompassing analgesic, antibacterial, anticancer, antifungal, antidiabetic, anti-inflammatory, antioxidant, mosquitocidal, antinociceptive, and antifertility effects. The biological properties are chiefly ascribed to the presence of diverse bioactive phytochemicals, including ricinine, gallic acid, quercetin, kaempferol-3-O-β-D-xylopyranoside, and quercetin-3-O-β-rutinoside [18]. The leaf extract contains flavonoids, phenolics, tannins, alkaloids, saponins, etc [19, 20].

Corrosion studies were performed on mild steel in sulphuric acid solutions both in the presence and absence of aqueous leaf extract fraction of *Ricinus communis* (RCAF). The efficacy of the extract as a corrosion inhibitor was studied using electrochemical techniques and the gravimetric method. Electrochemical tests were performed to study adsorption kinetics. The adsorption isotherms were used to determine thermodynamic parameters to explain the adsorption mechanism. The key constituents and functional groups within the aqueous extract were characterized by ultraviolet–visible (UV–Vis) spectroscopy, Fourier transform infrared (FTIR) analysis, and Gas chromatography–mass spectrometry (GC–MS). Surface characteristics, as well as the protective films on the metal, were assessed using Field-emission scanning electron microscopy with energy-dispersive X-ray spectroscopy (FE-SEM/EDX), atomic force microscopy (AFM), and X-ray photoelectron spectroscopy (XPS). Detailed thermodynamic and kinetic analyses involving the calculation of activation energy (E_a), activation enthalpy (ΔH^*), activation entropy (ΔS^*), and adsorption free energy (ΔG^o) were conducted to explain the adsorption behavior.

EXPERIMENTAL

Plant Collection and Preparation of Leaf Extract

Fresh *Ricinus communis* L. plants were collected from M992 + HHW Apple Ground Public Park, Narephat, Kathmandu 44600, Nepal, and the leaves were shade-dried. The dried

leaves were pulverised into a fine powder, extracted twice with hexane, and then air-dried. The powdered material was moistened with 25% ammonium hydroxide and kept for four hours to convert the basic salt (alkaloidal salt) into the bases. The material was then macerated in methanol for 72 hours and filtered. It was concentrated on a rotary evaporator (Model MVP 10 B SO22). To adjust the pH to 3–4 and convert the components into soluble salts, the concentrated extract was added to 5% HCl. The extract was partitioned with dichloromethane (DCM) solution. The aqueous phase had water-soluble salts after, whereas the other impurities were were in the organic phase. The aqueous phase was basified to pH 11-12 with 25% NH_4OH, which converted the salts back to their free bases. A second DCM partitioning was performed, and the DCM-insoluble (aqueous) fraction was collected and evaporated on a water bath [21, 22]. The resulting paste was used to study the corrosion inhibitor.

Preparation of the Mild Steel Sample and the Extract Solution

MS specimens were gathered from the local market in Bhaktapur. For gravimetric measurements and electrochemical studies, the metal samples used were 3 × 3 × 0.15 cm^3 and 2 × 2 cm^2, respectively. Every MS sample was polished using SiC abrasive papers up to 2000 grit, sonicated in ethanol for 15 minutes, and dried with a hot-air blower. The specimen was stored in a desiccator until further use.

Fisher Scientific H_2SO_4 (purity 98%, density 1.84 g/mL) was used to prepare the test solution. 1 M H_2SO_4 solution was prepared in distilled water. In this work, a 1000 ppm inhibitor extract solution was prepared in 1 M H_2SO_4, which was used as the stock solution. Different concentrations of inhibitor solutions were prepared by serial dilution of the stock solution in 1 M H_2SO_4.

Gravimetric Analysis (GA)

The known dimensions of the MS sample were weighed using a four-digit digital balance (BEL ENGINEERING model) and immersed in 75mL of acid solution, both with and without the RCAF. The experiment was carried out at various concentrations, times, and temperatures. The temperature was kept constant by a Clifton UNSTIRRED water bath. After reaching the desired time, the MS coupons were withdrawn, washed with distilled water using a brush, acetone, and dried. Finally, its weight was measured. Each experiment was performed three times, and the mean data were used. Using equations 1, 2, and 3, the corrosion rate (CR), surface coverage (θ), and inhibition efficiency (IE%) were calculated.

Corrosion rate (mm/y), $\mathrm{CR} = \frac{\Delta \mathrm{W} \times 87.6}{\mathrm{DAT}}$……(1)

Where ΔW=Weight loss in solution (mg), D=Density of MS, A=Surface area of MS immersed (cm^2), T= time of immersion (h)

Surface coverage, $\theta = (1 - \frac{\mathrm{CR}_2}{\mathrm{CR}_1})$……(2)

Inhibition Efficiency, $\mathrm{IE}\% = (1 - \frac{\mathrm{CR}_2}{\mathrm{CR}_1})$……(3)

Where CR_1 and CR_2 are the CRs of MS without and with RCAF.

Electrochemical Analysis

The Gamry Instruments Interface 1010™ was used to perform electrochemical measurements. Each experiment was conducted using the MS sample as the working electrode. Additionally, platinum was used as the counter electrode and a calomel electrode as the reference. Both in the absence and presence of RCAF, the electrolyte used was an 80 mL solution. After three hours of immersion, the open-circuit potential was measured, followed by electrochemical analyses.

Electrochemical Impedance Spectroscopy (EIS)

EIS experiments were carried out at open-circuit potential, applying a sinusoidal signal of 10 mV at a frequency range of 100 kHz to 0.01 Hz. Ten points were collected per decade. Inhibition efficiency was calculated using polarization resistance determined by measuring the diameter of the Nyquist semicircle as presented in Equation 4.

$IE\% = (1 - \frac{R_o}{R_p})$……(4)

Where R_o = polarization resistance of MS in acid,

R_p = polarization resistance of MS in acid and RCAF.

Potentiodynamic Polarization (PDP)

PDP was carried out within ±0.3 V of the open-circuit potential (OCP). The scanning rate of the electrode potential was 1 mV/s. The values of corrosion potential (Ecorr) and corrosion current density (icorr), as well as cathodic (βC) and anodic (βa) Tafel slopes, were determined by extrapolating the respective regions of the polarization plots. Using the icorr values for uninhibited and inhibited, IE was calculated using equation 5.

$$IE\% = (1 - \frac{i_{corr}}{i^0_{corr}}) \quad \text{.....(5)}$$

Where i^0_{corr} = the corrosion current density of MS in acid,

i_{corr} = the corrosion current density of MS in acid with RCAF.

Surface Analysis

The prepared metal samples were placed in a 1 M sulfuric acid solution for three hours, both with and without the inhibitor. Following the exposure, the samples were rinsed with distilled water and dried. The topographic and elemental characterization of the samples was performed using a Carl Zeiss SUPRA 55VP FESEM/EDX detector. Additional topographical information was obtained using an Agilent Technologies 5500 Series AFM. The chemical state of the surface-adsorbed inhibitor molecules was analyzed using X-ray photoelectron spectroscopy (XPS) with the ESCALAB 250 Xi instrument.

RESULTS AND DISCUSSION

Phytochemical Screening and Spectroscopic Analysis

Alkaloids were shown by phytochemical screening of RCAF as a standard protocol. Further, it was characterized by the following spectroscopic analyses.

Ultraviolet–visible (UV-Vis) Spectroscopic Analysis

UV–Vis spectroscopic analysis (SHIMADZU UV-3600 Plus) showed an absorption peak at 278 nm, as illustrated in Figure 1a. This indicates an n→π* electron transition and confirms the presence of heteroatoms and unsaturated organic compounds [23].

Fourier Transform Infrared (FTIR) Spectroscopic Analysis

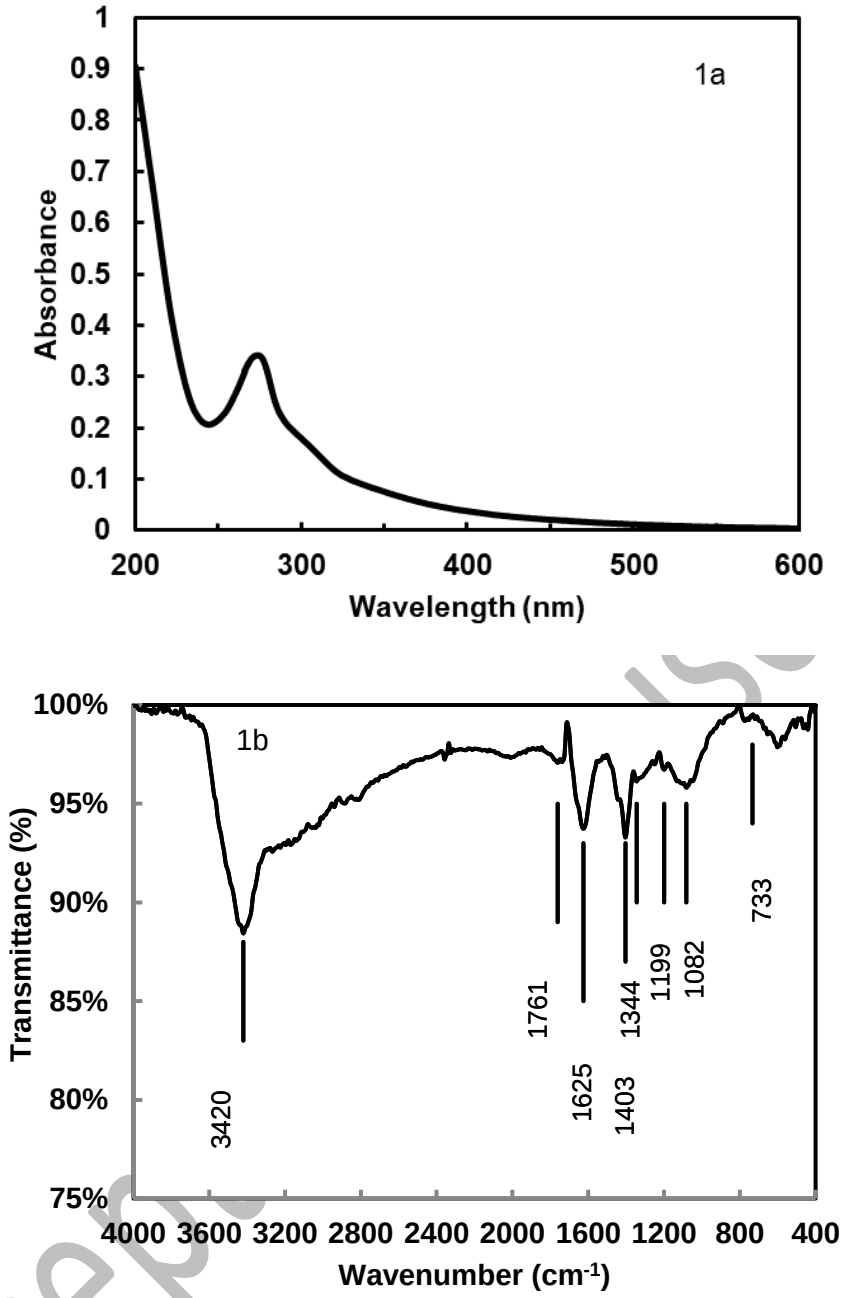

Fig. 1. a. UV-Vis and b. FTIR spectroscopy of RCAF.

The analysis of the FTIR spectrum of RCAF, recorded on a BRUKER TENSOR 27 and represented in Figure 1b, identified absorption bands and their possible functional groups, and is tabulated in Supplementary Table 1. The broad peaks at 3420 cm^{-1} represent the O–H stretching bands of alcohols and phenols, and can further be attributed to N–H stretching of amines or amides due to hydrogen bonding of the above functional groups. A typical feature at 1761 cm^{-1} is evidence for the stretching vibration of ester carbonyl groups, which implies the presence of carbonyl functionalities in the extract. The sharp peak at 1625 cm^{-1} is ascribed to C=C stretching of conjugated double bonds in aromatic rings or C=O bonds of amides, signifying the presence of aromatic or carbonyl groups in the extract. An absorption peak at 1404 cm^{-1} suggests bending vibrations of O-H groups in phenols or

alcohols and stretching vibrations of C-N bonds in amines. Similarly, a band at 1344 cm^{-1} signified the peaks of amine groups, alcohol or phenolic groups, or aliphatic CH_3 bending vibrations. Another band at 1199 cm^{-1} may be designated as C–O stretching in alcohols, ethers, and esters. The 1082 cm^{-1} and 733 cm^{-1} bands are due to stretching of C–O bonds in both alcohol and phenol functional groups as well as C–N stretching and aromatic C–H out-of-plane bending, respectively [24].

Gas chromatography–mass spectrometry (GC–MS)

The mass spectra given by GC-MS in RCAF are shown in Figure 2. Nitrogen-containing compound identified by GC-MS were m-methoxybenzonitrile, 5H-tetrazol-5-amine, ethylamino-1-propylcyclohexane, 1-Methyl-2,5-dipropyldecahydroquinoline, Recinine, 4-(5-Ethyl-1,2,4-oxadiazol-3-yl)benzoic acid, and 1-Norvaline N-methoxycarbonyl-nonyl ester.

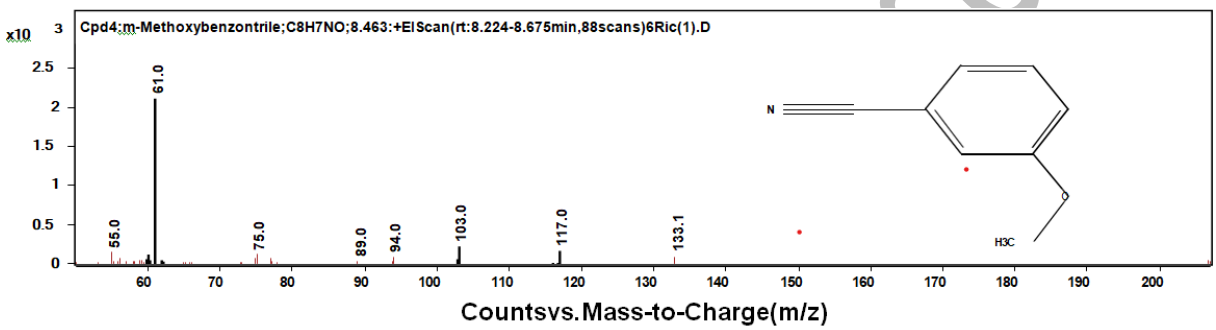

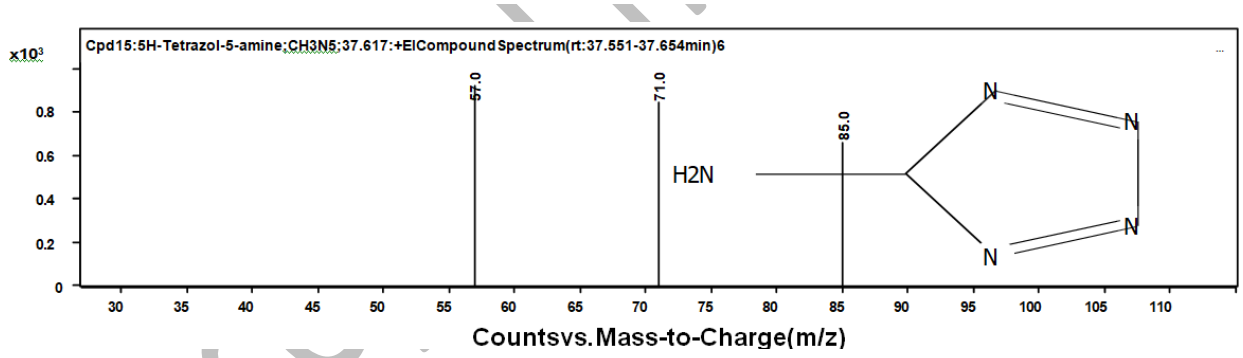

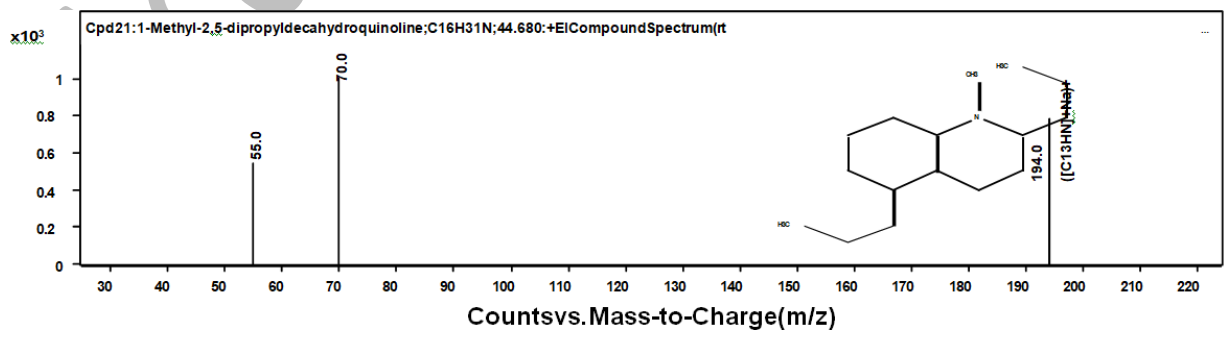

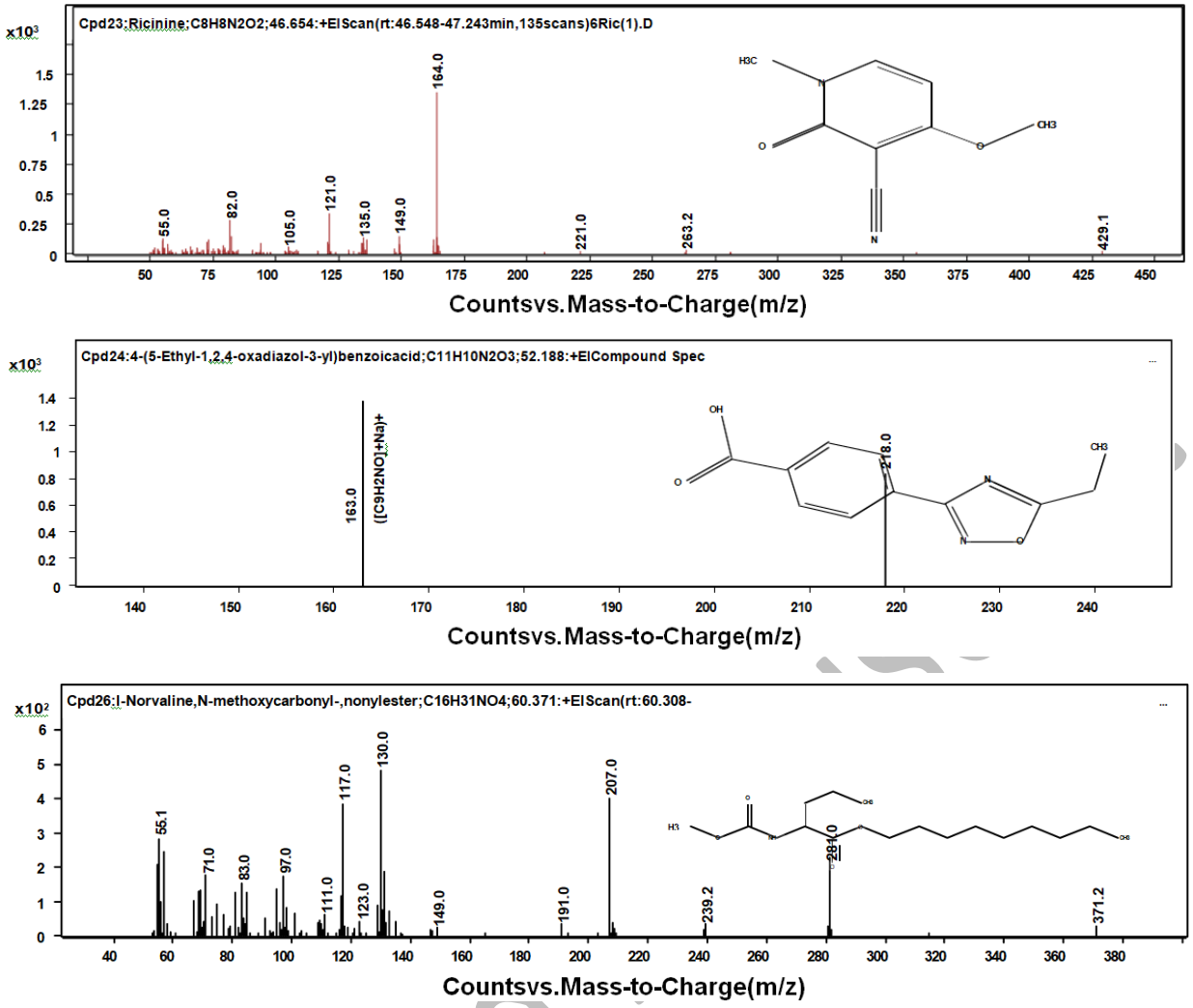

Fig. 2. GC-MS Mass fraction of N-containing compounds in the RCAF.

Gravimetric Analysis (GA)

The gravimetric analysis (GA) was used to study the effects of immersion time, inhibitor concentration, and temperature on the corrosion rate (CR) of the MS sample.

Effect of Time

GA was carried out for varying immersion times of MS samples, namely 0.5 h, 3.0 h, 6.0 h, and 24.0 h. As the concentration of the inhibitor increased, a progressive reduction in the rate of corrosion of mild steel (Figure 3a). Correspondingly, the inhibition efficiency enhanced (Figure3b). The least weight loss occurred at 300 ppm (Figure 3c). This decrease in CR and increase in IE with increased RCAF concentration may be attributed to the absorption of RCAF molecules onto the MS surface.

At 300 ppm, the highest inhibition efficiency (IE) was observed after 3 h, whereas at 100 ppm, it was observed after 0.5 h. The lower concentration of RCAF results in fewer molecules, which are quickly adsorbed onto the metal surface, forming a protective layer.

This process enhances the inhibition efficiency. However, at higher concentrations, the adsorption process required a longer time to reach equilibrium due to higher molecules. After a certain immersion period, desorption of the inhibitor began, leading to a gradual decrease in IE.

Calculated values of CR, IE, and weight loss for tested concentrations are given in the Supplementary Table.

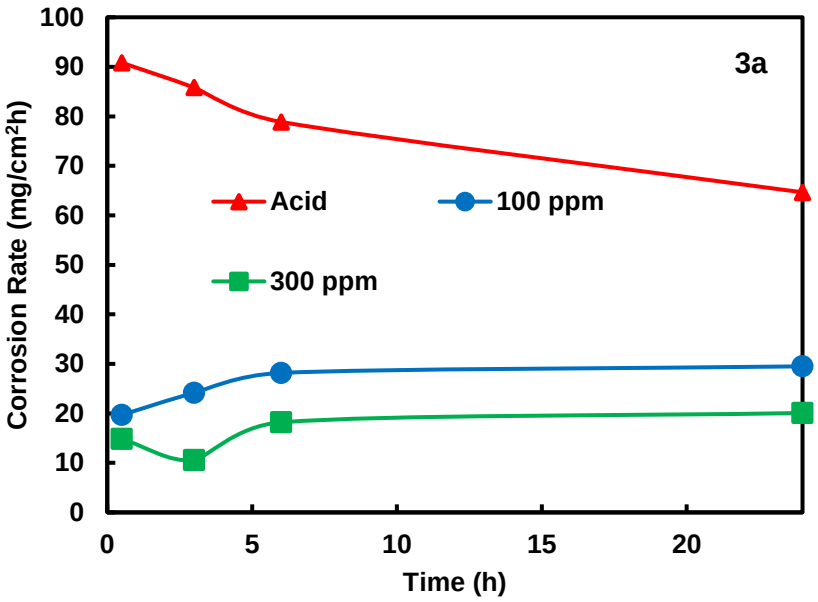

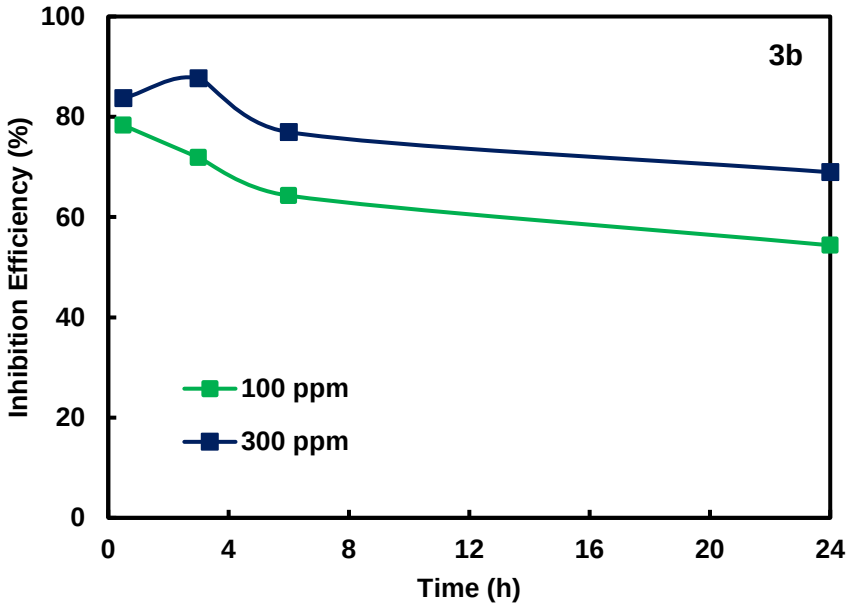

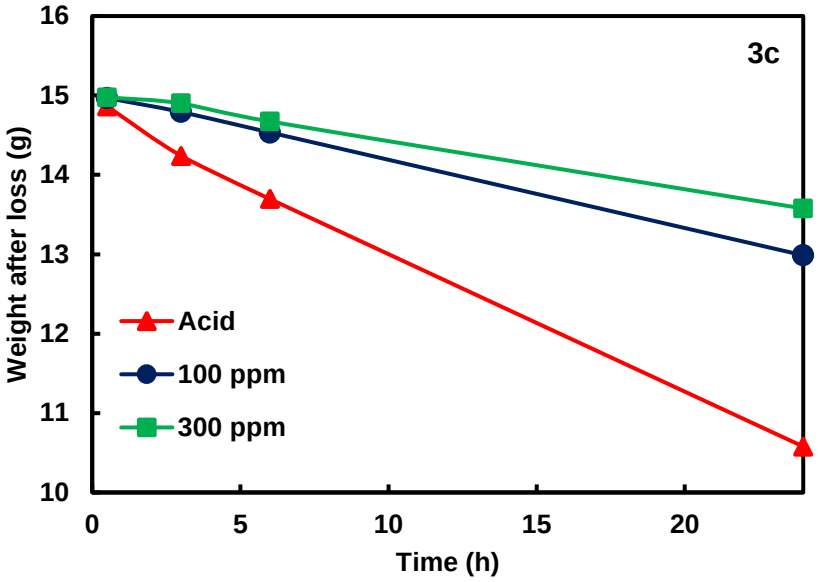

Fig. 3. (a) Corrosion rate, (b) Inhibition efficiency, and (c) Weight after loss of MS at various times

Effect of Concentration

The weight of the metal sample was measured before and after 3 hours of immersion in the acid solution at 303 K. Experiments were done for the blank sample (uninhibited) and for a solution with 100, 150, 200, 250, 300, and 350 ppm of the RCAF, according to Supplementary Table 4. Figure 4 illustrates the effect of inhibitor concentration on CR and IE. The CR value declined continuously with increasing concentrations of RCAF. At the same time, the IE value increased. The main reason is the adsorption of RCAF molecules on the MS surface, which shields against corrosion.

The methanolic extract of *Berberis aristata* at 1000 ppm attained 98.18% corrosion inhibition [25]. Similarly, the ethanolic extract of *Ruta chalepensis* exhibited 87.00% coprrosion inhibition at a concentration of 3.5 g/L [26]. Furthermore, the aqueous extract of *Morinda tinctoria* leaves on aluminum showed an inhibition efficiency of 74.06% at 7% extract concentration [27]. In addition, nano-carbon made from waste mango kernels was 87.10% effective at 800 ppm [28].

In this study, 87.70% IE was achieved for RCAF at 350 ppm. Thus, the aqueous fraction of *Ricinus communis* L. extract can be regarded as an excellent corrosion inhibitor.

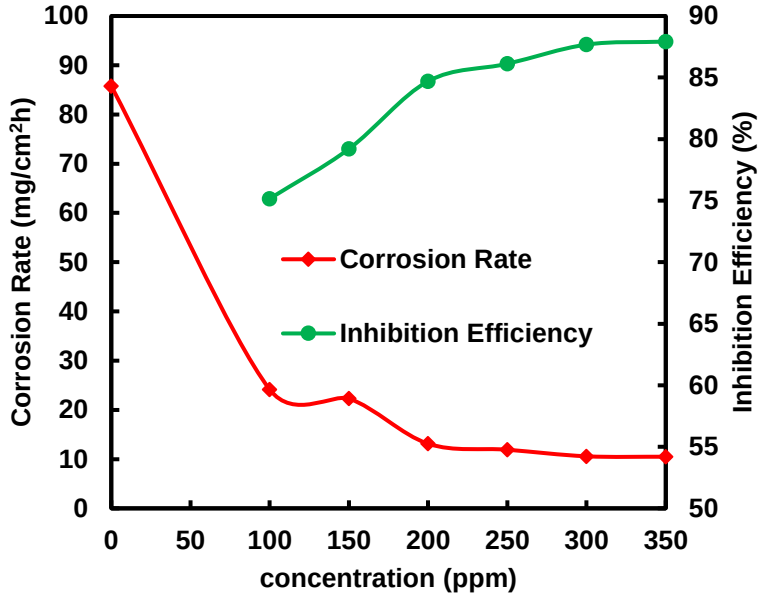

267

Fig. 4. Variation of CR and IE with various concentrations of RCAF.

Effect of Temperature

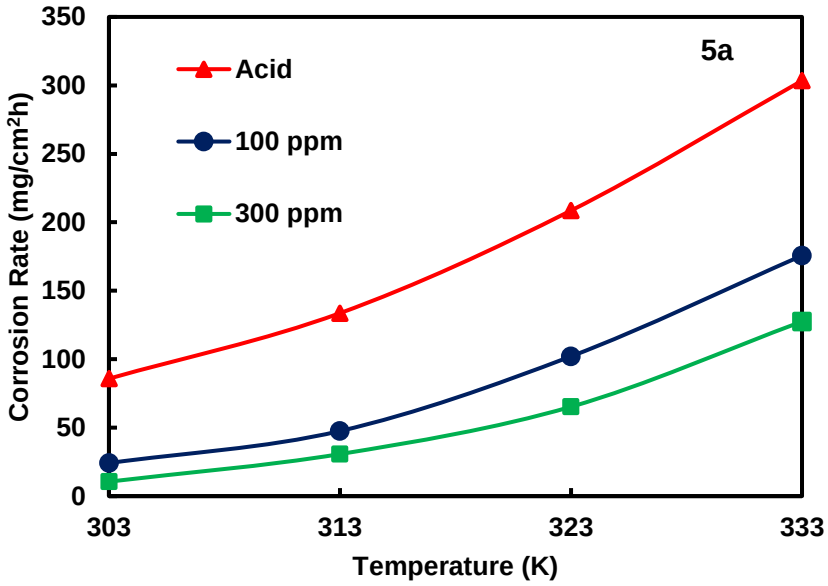

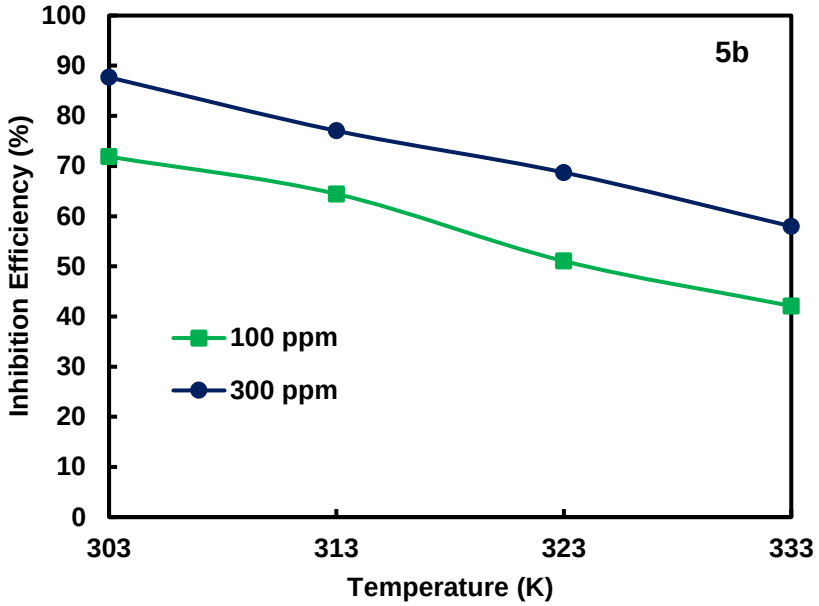

Fig. 5. (a) variation of CR and (b) IE with Temperature.

Table 1. Corrosion rate and Inhibition efficiency at various temperatures.

Concentration (ppm)	Temperature (K)	Corrosion Rate (mm/yr)		Inhibition Efficiency(%)
		Acid	Acid + Inhibitor	
100 ppm	303	85.80	24.13	71.87
	313	133.66	47.54	64.43
	323	208.56	102.08	51.05
	333	303.43	175.70	42.10
300 ppm	303	85.80	10.57	87.68
	313	133.66	30.71	77.02
	323	208.56	65.26	68.70
	333	303.43	127.60	57.97

The effect of temperature on corrosion for uninhibited and inhibited MS samples after an immersion of 3.0 hours. The study was conducted at inhibitor concentrations of 100 ppm and 300 ppm, at 303 K, 313 K, 323 K, and 333 K. The temperature investigation also showed that raising the concentration of RCAF successfully decreased the corrosion rate of mild steel (Figure 5a) (Table 1) The IE reached its highest value at 303 K for both 100 ppm and 300 ppm concentrations (Figure 5b). An increase in temperature increases the kinetic energy of surface atoms, reducing the adsorption of inhibitory species on the metal surface, causing desorption. Thus, the adsorption–desorption equilibrium would shift toward desorption, as shown in equation 6 [29].

$$\boldsymbol{Adsrption} \rightleftharpoons \boldsymbol{Desorption} \quad \text{.....(6)}$$

Adsorption Isotherm

Of all the adsorption models considered, the Langmuir isotherm was the most accurate one with respect to the GA. This is due to the high correlation coefficient (R^2 = 0.99925) and the

slope being close to unity (Figure 6). The small variation in the value of R^2 from unity can be attributed to the interaction of RCAF molecules with the MS surface. It could result from mutual attractions and repulsions among the adsorbed molecules [5]

The Langmuir adsorption isotherm is given as equation 7.

$$\frac{C_{inh}}{\theta} = C_{inh} + \frac{1}{K_{ads}} \text{.....(7)}$$

Where C_{inh} is the average molar concentration of RCAF and □ is the surface coverage, K_{ads} is equilibrium constant of adsorption

The standard free energy of adsorption (ΔG°_{ads})is calculate using equation 8.

$$\Delta G^{0}_{ads} = -RTln(55.5K_{ads}) \text{.....(8)}$$

Where 55.5 is the molar concentration of the solution in water

R = gas constant, and T = absolute temperature.

The spontaneous nature of the adsorption process of RCAF on the surface of MS is evident from the negative value of ΔG°ads. Generally, a value of ΔG°ads close to −20 kJ/mol indicates that the type of adsorption process taking place is physical adsorption due to electrostatic attraction, while a value equal to or less than −40 kJ/mol implies chemical adsorption with charge transfer or electron transfer [30]. The calculated ΔG^{o}_{ads} Value of −32.30 kJ·mol^{-1} indicated that the inhibitor undergoes both physical and chemical adsorption.

The activation energy (E_a) can be calculated from the Arrhenius equation (9) as

$$logCR = logA - (\frac{E_a}{2{,}303}) \text{.....(9)}$$

Where CR is the corrosion rate, A is the Arrhenius pre-exponential constant, Ea is the apparent activation energy, R is the universal gas constant, and T is the absolute temperature.

The thermodynamics of corrosion in terms of enthalpy and entropy were obtained from the transition state equation formulated in Equation 10 below.

$$\log\left(\frac{CR}{T}\right) = \left[\log\left(\frac{R}{hN}\right) + \left(\frac{\Delta S^*}{2.303R}\right) - \frac{\Delta H^*}{2.303RT}\right] \text{.....(10)}$$

Here, ΔH* is the activation enthalpy, ΔS* is the activation entropy, R is the universal gas constant, T is the absolute temperature, h is Planck's constant (6.6261×10^{-34} J s), and N is Avogadro's constant (6.0225×10^{23} mol^{-1}) [5].

Table 2. Thermodynamic parameters for the MS sample in acid without and with extract.

Inhibitor	E_a (kJ/mol)	ΔH*(kJ/mol)	ΔS* (J/molK)	E_a-ΔH*(kJ/mol)
Blank	35.54	32.91	-99.47	2.64
100 ppm	56.42	53.78	-41.15	2.64
300 ppm	69.17	66.53	-5.23	2.64

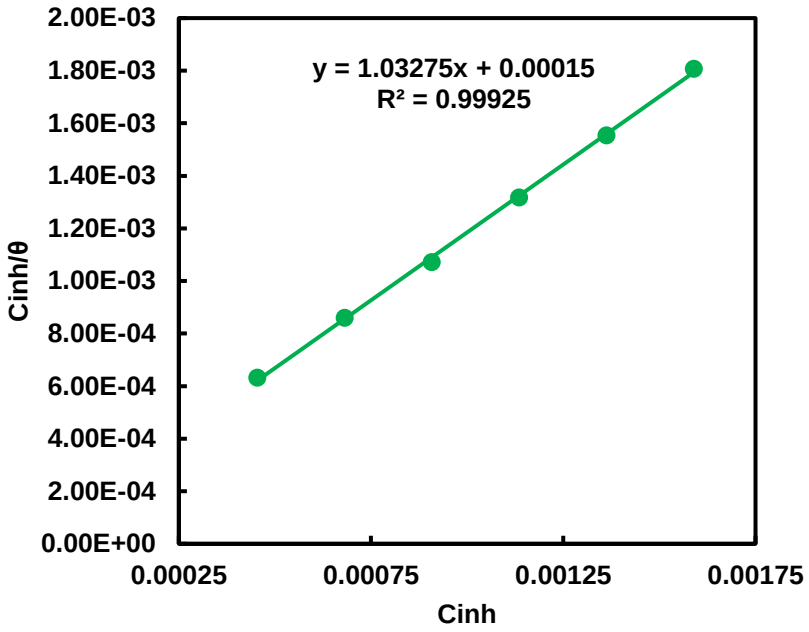

Fig. 6. Langmuir adsorption isotherm

The Arrhenius plot (Figure 7a) and the transition state plot (Figure 7b) reveal a rise in both E_a and ΔH*, due to the addition of RCAF. The thermodynamic activation parameters are determined from the Transition state plot; that is, ΔH* is estimated from the slope while ΔS* is estimated from the intercept, and shown in Table 2.

The positive value of ΔH* indicating the endothermic process. The elevated activation enthalpy (ΔH) on addition of the inhibitor suggests that the corrosion mechanism is primarily governed by activation-controlled kinetics [17]. It may be further deduced from the fact that Ea > ΔH*, indicating the evolution of gas during the course of corrosion, particularly the cathodic evolution of hydrogen [31]. The difference measured between activation energy and activation enthalpy was 2.64 kJ mol^{-1}, which was close to the RT value. This clearly indicated that the corrosion process followed a unimolecular mechanism and was consistent with the ideal gas equation [5, 32].

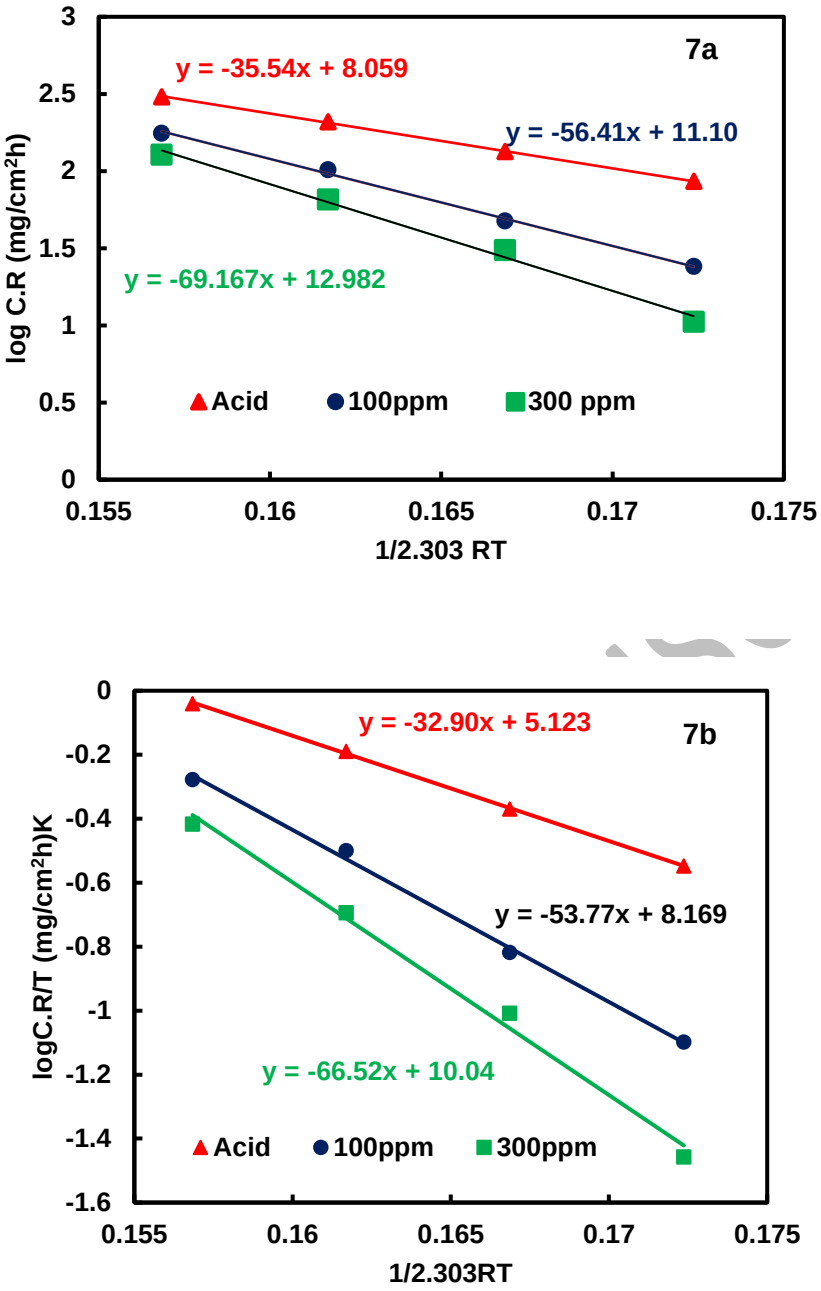

Fig. 7. (a) Arrhenius Plot and (b) Transition state plot of MS in acid and RCAF in acid.

The increase in ΔS* with increasing RCAF concentration indicates an increase in randomness in the system as it goes from the initial to the activated state. This is due to the displacement of water molecules from the metal surface and the adsorption of the inhibitors [33].

Electrochemical Measurements

Electrochemical Impedance Spectroscopy (EIS)

Figure 8a illustrates the measured OCP. There is a slight positive shift in the OCP in the presence of RCAF. This can be attributed to the adsorption of RCAF molecules onto the mild steel surface and the consequent formation of a protective barrier film. The variation in

the OCP value <85 mV shows that RCAF can be classified as a mixed-type inhibitor [34, 35].

This technique measured the effect of RCAF concentration (C_{inh}) on the impedance behavior of MS in an acidic medium. The corresponding Nyquist and Bode plots are presented in Figures 8a and 8b. The experimental impedance data are presented as symbols, while the fitted data obtained using Zview 2.0 software are represented by a solid line. Figure 10a and Figure 10b represent the equivalent circuit model used to fit the data.

Figure 8b shows the measured impedance spectra. A single relaxation loop was observed in all Nyquist plots. This indicates the corrosion process is governed by the basic mechanism in both the uninhibited and inhibited (RCAF) solutions. There is a depressed (not perfect) semicircle in Nyquist Plots, with centers lying below the real axis. This behavior is due to surface heterogeneity and roughness on solid electrodes [34, 36]. To consider the deviations from ideal capacitors, a constant phase element (CPE) is used instead of the ideal double-layer capacitor (Cdl). The impedance of a CPE is characterized by the following equation 11.

$$Z_{CPE} = Y_o^{-1}(iw)^{-n} \quad (11)$$

The double layer capacitance (C_{dl}) related CPE by equation (12)

$$C_{dl} = (Y_o R_n^{n-1})^{-n} \quad (12)$$

Where, Y_o represents CPE constant, w denotes the angular frequency of the sinusoidal disturbance, $i^2 = -1$ is an imaginary number, and n = a/π/2. Here, α is the phase angle of the CPE, whereas n is the CPE exponent ($0 \le n \le 1$). The CPE exponent indicates how much the capacitor deviates from being ideal, and is an indication of the surface roughness [37].

The polarization resistance (diameter of the semicircle), R_p, is the sum of the charge-transfer resistance, R_{ct}, the diffusion resistance, R_d, and the resistance due to the corrosion product layer on the surface, R_a. With the addition of RCAF, another contribution arises from the adsorbed organic film and possible metal–organic complex formation (R_f). Thus, the total resistance can be presented as: $R_p = R_{ct} + R_d + R_a + R_f$ [35].

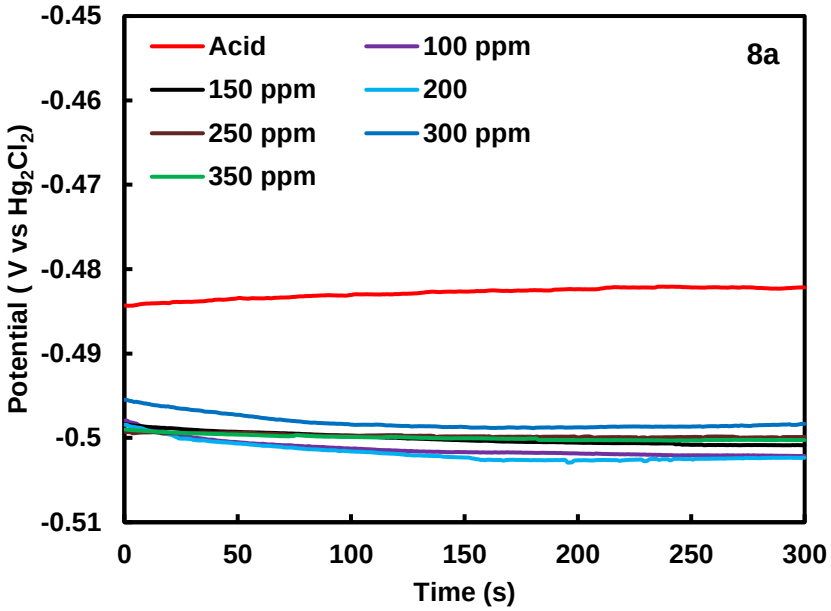

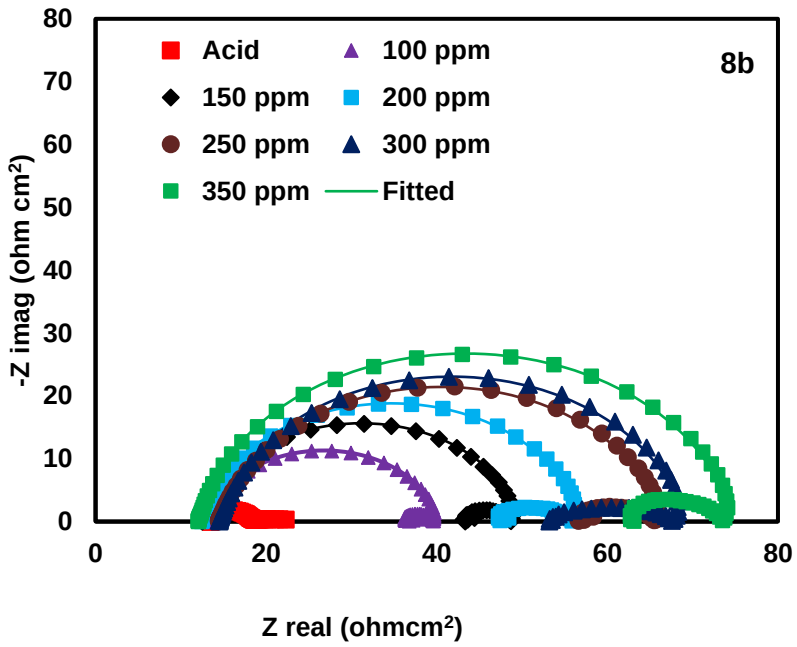

Fig. 8. a. OCP and b. Nyquist Plot for MS in acid without and with RCAF

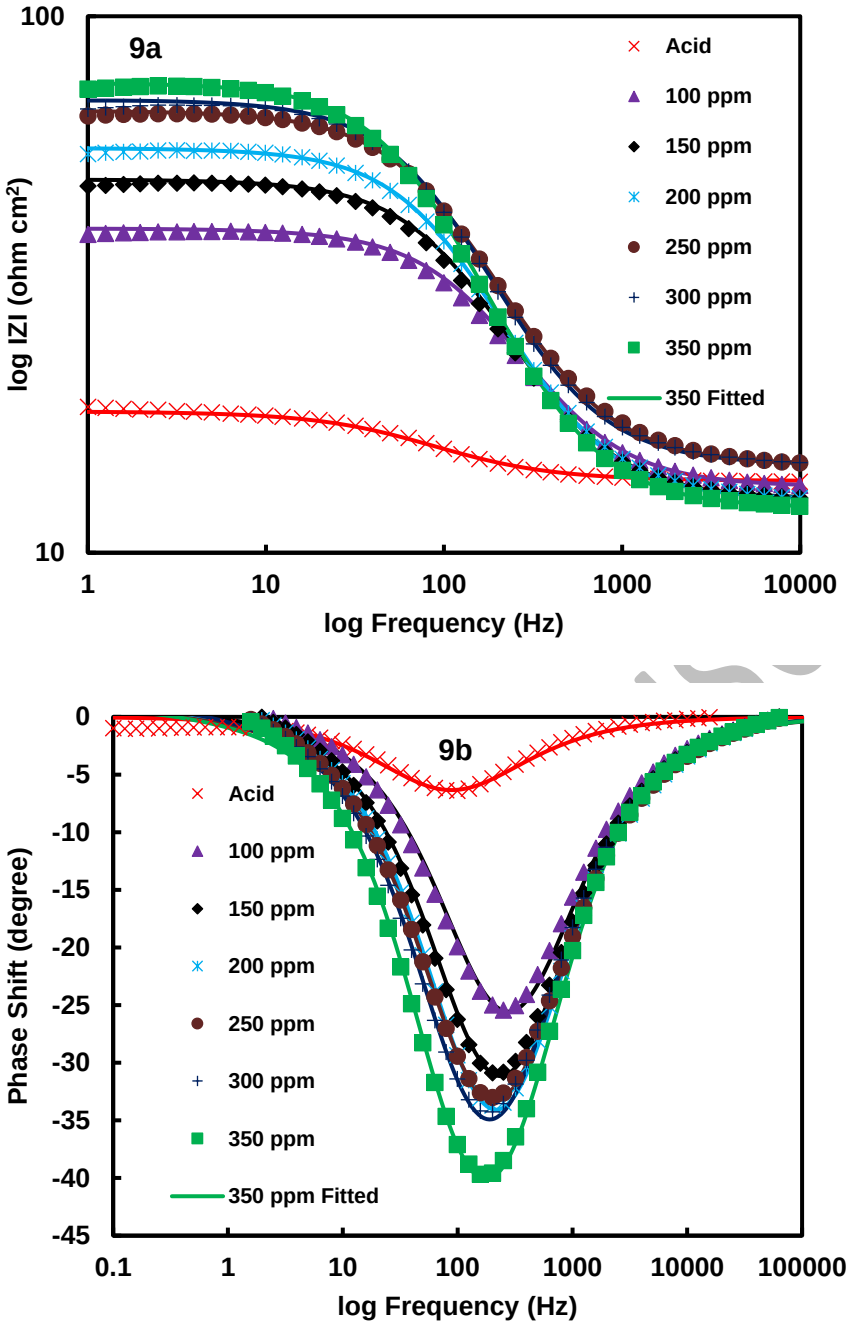

Fig. 9. a. Bode plot and b. Phase shift for MS in acid without and with RCAF

Polarization resistance (R_p) increases progressively with RCAF concentration. This is due to the formation of a barrier film on the surface of the mild steel caused by the adsorption of RCAF molecules, which prevents corrosion. As the concentration of RCAF molecules increased, the value of CPE decreased because more RCAF molecules were occupying the active sites of the metal through the replacement of the adsorbed water molecules. The higher the surface coverage, the thicker the protective layer formed, which in turn reduced the corrosion rate [38]. Additionally, corrosion products present on the surface form a loose coating that further helps inhibit corrosion [39].

10a 10b

Fig. 10. The Equivalent Circuit Model used to fit EIS data (a) Acid and (b) Acid +RCAF

As shown in Table 3, the inhibition efficiency (IE) increased progressively with inhibitor concentration and attained a maximum value of 92.17% (350 ppm) based on electrochemical impedance spectroscopy (EIS). An inductive loop was observed in all Nyquist spectra in the low-frequency regime. This kind of behavior is usually associated with the adsorption and relaxation of intermediate corrosion products at the metal/acid solution interface, such as $[FeSO_4(ads)^{2-}]$ and $[FeOH]^-$. The formation of the inductive loop at rising RCAF concentrations suggests the development of a more pronounced metal-RCAF complex on the surface of mild steel, hence the formation of a protective adsorbed film. The adsorption and desorption of RCAF molecules attain a dynamic equilibrium [40].

Table 3. Electrochemical impedance parameters of MS in acid and acid + RCAF

Concentration (ppm)	Rs (Ωcm^2)	Y_o	n	R_{ct} (Ωcm^2)	R_f (Ωcm^2)	L (Ωcm^2)	$R_P=R_{Ct}+R_f$ (Ωcm^2)	IE (%)
Blank	15.4	0.001475	0.771	4.94	-	-	4.94	
100	13.25	8.56E-05	0.888	26.20	0.80	0.70	27.00	82.00
150	12.57	7.95E-05	0.892	36.00	1.10	1.20	37.10	86.68
200	12.53	7.49E-05	0.896	43.32	1.00	1.00	44.32	88.85
250	14.53	7.58E-05	0.877	51.00	1.20	1.20	52.20	90.54
300	14.55	7.178E-05	0.890	53.44	2.00	1.07	55.44	91.10
350	12.5	7.18E-07	8.899	61.6	1.50	1.50	63.10	92.17

Figures 9a and 9b present Bode plots and phase angle diagrams, respectively, that exhibit a single time constant and are thus in good agreement with the single capacitive loop observed in their Nyquist plots. This behavior confirms that the corrosion reaction occurs mainly through charge transfer and does not affect the metal dissolution mechanism. Similarly, the phase angle profile shows the uniformity and stability of the protective layer adsorbed on the metal surface [41].

Potentiodynamic Polarization (PDP)

The kinetics of reactions were assessed using PDP measurements of MS in bare acidic solution and in the presence of RCAF. The corresponding curves are given in Figure 11. The evaluated electrochemical kinetic parameters include the corrosion current density

(i_{corr}), corrosion potential (E_{corr}), and the anodic (β_a) and cathodic (β_c) Tafel slopes, which
405 are compiled in Table 4. The percentage of IE was determined by linear extrapolation of the polarization curves. The values of β_a and β_c give information on the electrochemical kinetics of the corrosion processes.

408 A decrease in the current density of the polarization curve was observed on the addition of RCAF, while the corrosion potential (E_{corr}) exhibited minimal variation. This behavior suppressed both the anodic dissolution of mild steel and the cathodic hydrogen evolution
411 reaction. In addition, there were only slight variations in the corrosion potential (Ecorr) between systems with and without the inhibitor, while the Tafel slopes (βa and βc) were almost constant. This shows that the RCAF works as a mixed-type corrosion inhibitor. The
414 maximum inhibition efficiency (92.57%) was recorded at 350 ppm

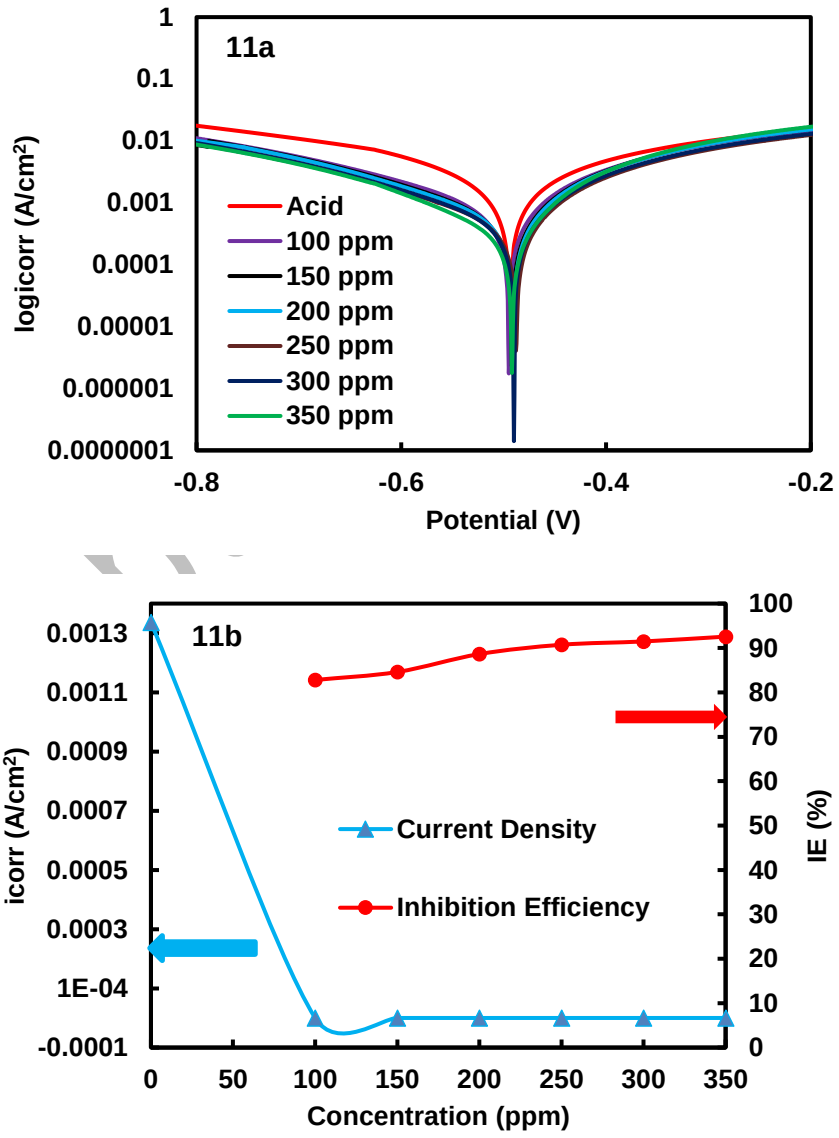

Fig. 11. (a) Potentiodynamic polarization for MS in acid without and with RCAF, and (b) IE and i_{corr}
417 with the concentration of RCAF.

Table 4. Potentiodynamic polarization parameters for MS I acid and acid + RCAF.

Concentration (ppm)	$-E_{corr}$ (V/SCE)	I_{corr}(Acm^{-2})	βa (V/dec)	-βc(V/dec)	IE %
Acid	0.492	1.33×10^{-3}	0.0136	0.185	
100	0.494	2.30×10^{-4}	0.063	0.114	82.80
150	0.493	2.06×10^{-4}	0.064	0.119	84.60
200	0.490	1.52×10^{-4}	0.022	0.13	88.63
250	0.487	1.24×10^{-4}	0.049	0.093	90.73
300	0.489	1.14×10^{-4}	0.0173	0.076	91.47
350	0.491	9.95×10^{-5}	0.020	0.077	92.57

MORPHOLOGICAL STUDY (SURFACE CHARACTERIZATION)

Field Emission Scanning Electron Microscopy with Energy Dispersive X-ray Photo-Spectroscopy (FE-SEM/EDX)

The surface topography and chemical composition of MS samples under acidic environments with and without RCAF were analyzed using FE-SEM and EDX (Figure 12). It was observed that the RCAF-treated sample has relatively smoother surfaces (Figure 12b), while the EDX analysis confirmed the presence of C, N, O, and S (Figure 12d). Conversely, the surface of the uninhibited sample was found to be severely attacked, exhibiting pores and cracks (Figure 12a); accordingly, its EDX analysis confirmed the presence of only C, O, and S (Figure 12c). The presence of S can be explained by the fact that both samples were treated with H_2SO_4 solution. These results provide conclusive evidence of RCAF molecule adsorption on the MS surface, forming a protective barrier layer that suppresses the corrosion reaction.

12a

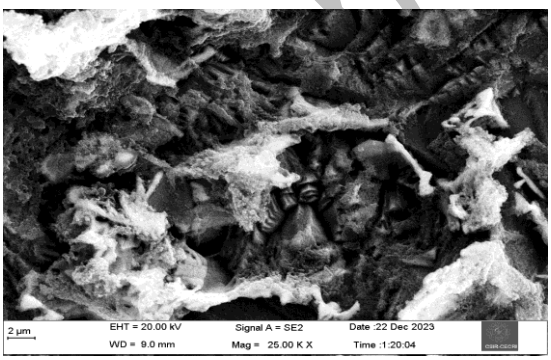

12b

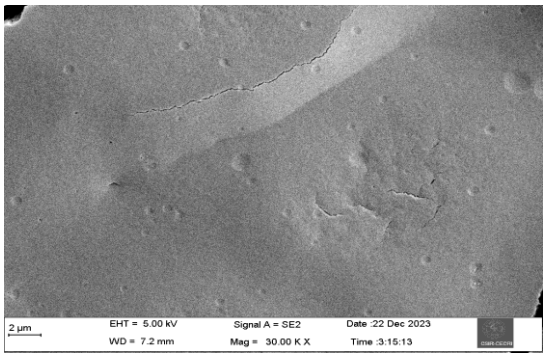

12c 12d

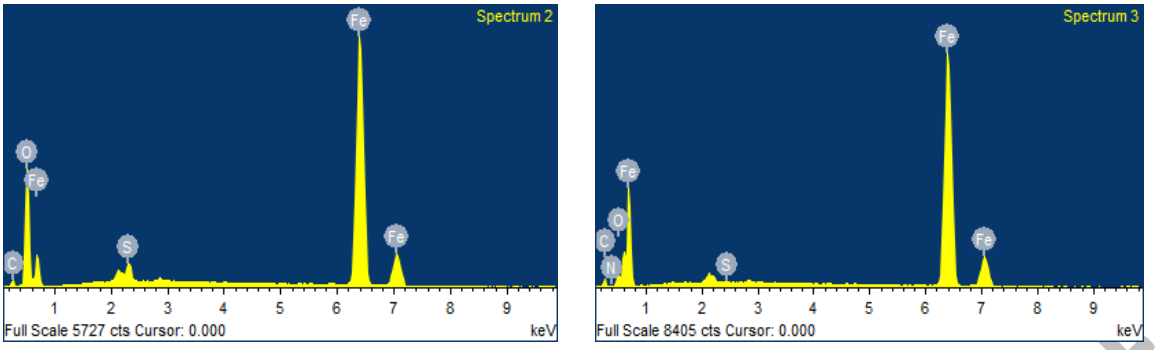

Fig. 12. Fe-SEM of (a) uninhibited MS, (b) Inhibited and (c) EDX of uninhibited MS, (d) Inhibited

435

Atomic Force Microscopy (AFM)

The surface topography of MS specimens was investigated using atomic force microscopy
438 (AFM). As shown in Figure 13, the corroded sample exhibited a highly irregular surface with pronounced peaks in both 2D (Figure 13d) and 3D (Figure 13e) images, indicating intense corrosion by the acidic medium. In contrast, the MS surface treated with the inhibitor
441 appeared significantly smoother in both 2D (Figure 12a) and 3D (Figure 12b) images. The corresponding topographic scale is presented (Figure 13c and Figure 13f). As confirmed by AFM data, a significant decrease in the surface roughness parameters was noticed; in
444 particular, the total height of the roughness profile (R_t) decreased from 0.561 µm to 0.464 µm, and the arithmetic average roughness (R_a) decreased from 0.101 µm to 0.0711 µm. These data further confirm the development of a protective layer that minimized the
447 dissolution of the metal surface [42].

13a 13d

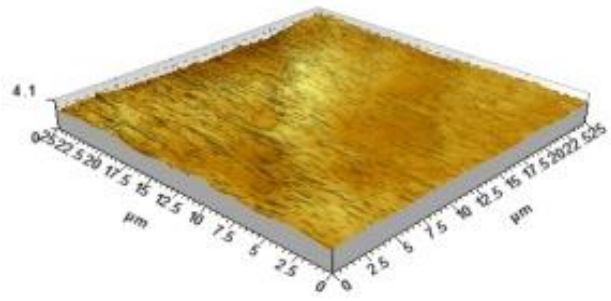

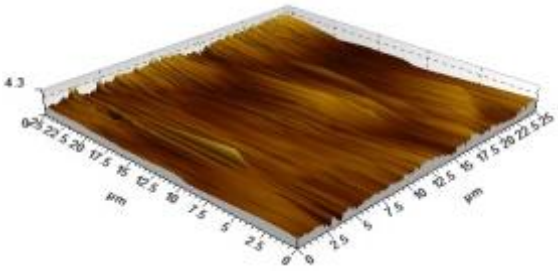

13b 13e

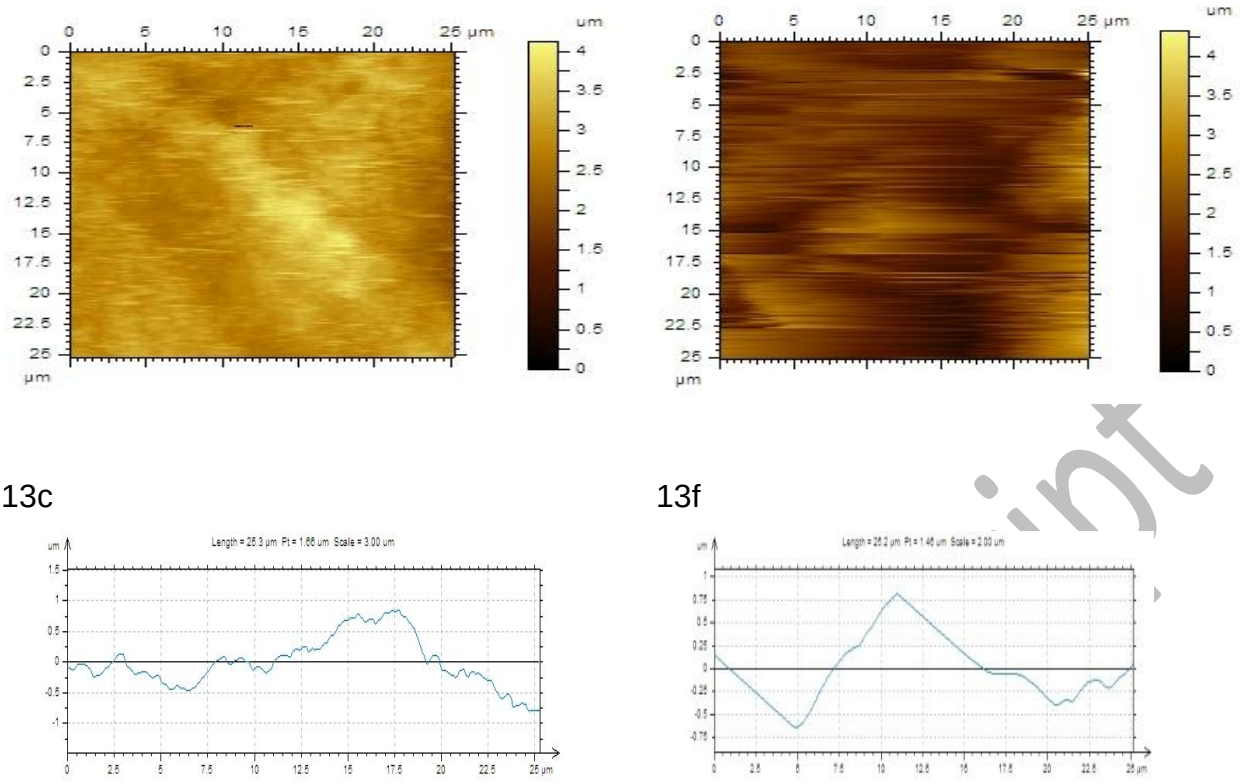

Fig. 13. AFM of Inhibited (a)-3d, (b)-2d, and (c)-topographic measurement, Uninhibited (d)-3d, (e)-2d, and (f)- topographic measurement

X-ray Photoelectron Spectroscopic Studies (XPS) of the Inhibited MS Surface

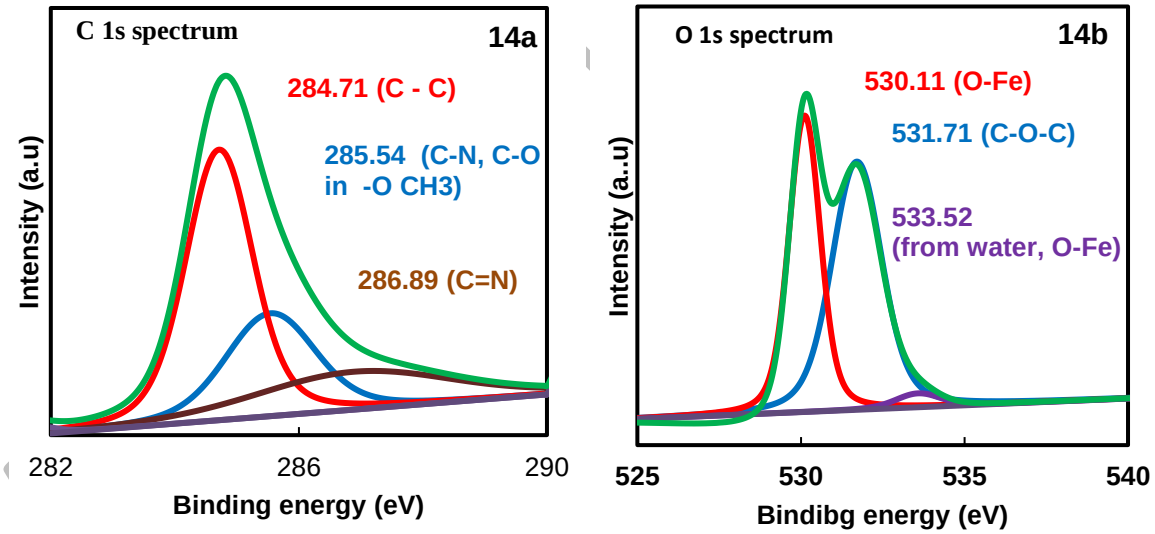

14a

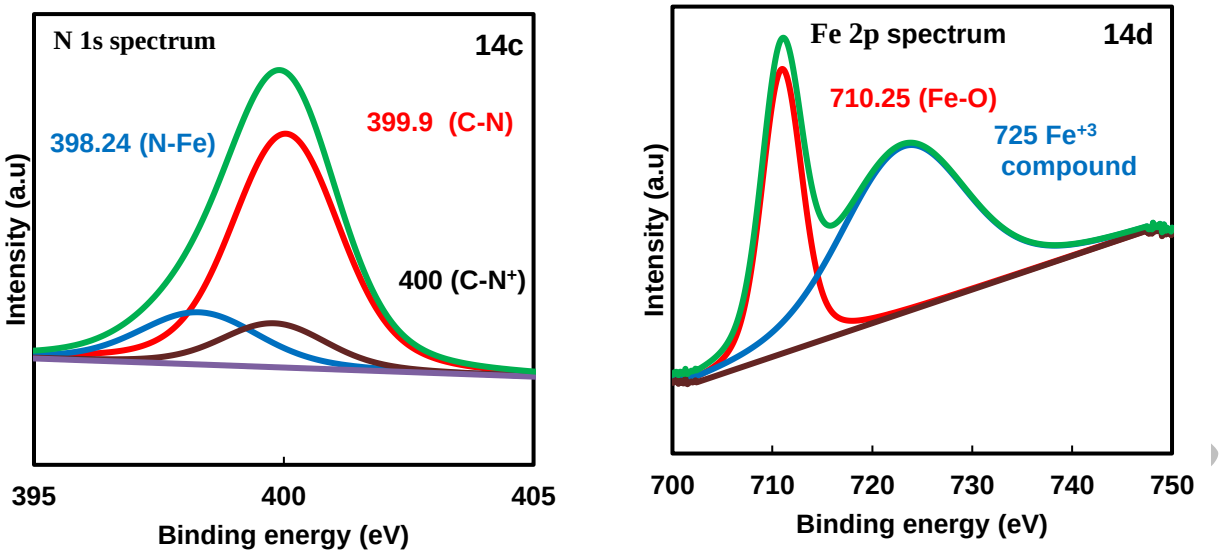

Fig. 14. XPS spectrum of inhibited MS sample a. Carbon, b. Oxygen, c. Nitrogen and d. Iron.

The XPS survey spectrum confirmed the signals of C 1s, O 1s, N 1s, and Fe 2p on the surface of MS. The deconvolution of the individual spectra was carried out using the Casa XPS software. The three major peaks from the C 1s spectrum at 284.71 eV, 285.54 eV, and 286.89 eV are attributed to the C–C/C–H, C=O/C–N, and C–N/C–N^+ groups, respectively, as shown in Figure 14a. The O 1s showed three components at 530.11 eV, 531.71 eV, and 533.52 eV, corresponding to the O–Fe bonds, C–O groups, and oxygen from adsorbed water, respectively (Figure 14b). Similarly, the N 1s spectrum exhibits three peaks at 398.24 eV due to Fe–N, 399.90 eV due to N–C, and 400.00 eV due to C–N^+, as presented in Figure 14c. The peaks at 710.25 eV and 725.00 eV are assigned to Fe $2p_3/_2$ and Fe $2p_1/_2$, respectively. Deconvolution further pointed out components at approximately 711 eV, which is fitted to Fe–O, and 707 eV assigned to the metallic Fe^0, whereas the peak at 725 eV is associated with Fe^{3+} species (Figure 14d) [10, 43, 44]

Corrosion Inhibition Mechanism

Inhibition of corrosion occurs as a result of the adsorption of the inhibitor molecules on the MS surface. The thermodynamic calculations indicate that adsorption occurs via a two-step mechanism. Initially, both the MS surface and the RCAF molecules present in the solution carry positive charges. The positively charged MS surface, therefore, gets attracted to the negatively charged SO_4^{2-} ions present in the acidic solution. This process facilitates the adsorption of RCAF molecules, particularly at the cathodic sites, where the hydrogen evolution reaction is inhibited.

In the RCAF molecules, there are lone pairs present in the HOMO, which can transfer electrons to fill the empty d-orbitals of the metal, forming a coordinate bond. Consequently, adsorption occurs at anodic sites, which helps prevent metal dissolution [45]. As adsorption

proceeds, the MS surface becomes negatively charged. In order for the system to be neutral, back-donation of electrons (retro-donation) begins from the 4s orbital of the metal to the lowest unoccupied molecular orbital (LUMO of the RCAF molecules [17].

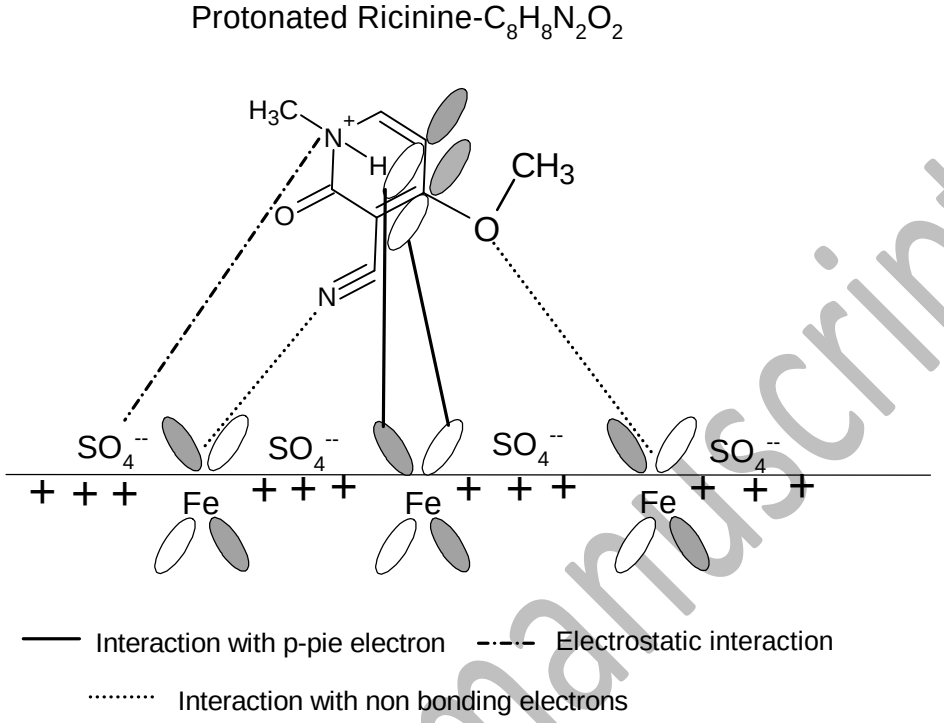

Fig. 15. Schematic representations of the adsorption of protonated Ricinine – $[C_8H_8N_2O_2]^+$ion MS.

In Figure 15, it can be seen that the adsorption of Protonated Ricinine on the MS surface includes the synergistic effect of the sulfate ions.

CONCLUSIONS

Ricinus communis aqueous fraction leaf extract (RCAF) showed high corrosion inhibition efficiency, reaching 92.57% at 350 ppm and 303 K. The smoother surface morphology in the FE-SEM images of the inhibited sample provide clear evidence for the adsorption of RCAF molecules and the formation of a protective barrier film on the mild steel surface. AFM results supported this observation by showing a significant decrease in the total height of the roughness profile of the MS surface, with Rt values reduced from 0.561 µm (without inhibitor) to 0.464 µm (with inhibitor), and the arithmetic average deviation (Ra) decreased from 0.101 µm to 0.0711 µm. XPS analysis further confirmed the adsorption mechanism through the interaction of C 1s, O 1s, and N 1s species from the extract with Fe 2p, indicating the formation of a stable protective film on the inhibited steel surface. The inhibition efficiency is mainly due to the adsorption of heteroatom-containing molecules on the mild

steel surface. Efficiency increased with concentration but decreased with higher temperature and longer immersion time (3 h). Adsorption follows the Langmuir adsorption isotherm, suggesting monolayer adsorption. Thermodynamic parameters (Ea and ΔH*) suggest a mixed-mode adsorption (physical + chemical) and a unimolecular, kinetically controlled process. EIS results showed a single time constant, meaning the reaction mechanism remained unchanged. Collectively, the results demonstrate that RCAF provides effective corrosion protection and represents a promising environmentally benign inhibitor for mild steel in acidic conditions

FUNDING

The research study has been supported by the TU Janasakti Bikash Tatha Kalyan Program, Coordination Division, Office of the Rector, Tribhuvan University, Nepal, Grant Number 83/081/082. Further support has been provided to this study by the India Science and Research Fellowship (ISRF) Program, Award Number INSA/DST- ISRF/2023/NEP/06/.

ACKNOWLEDGMENTS

The author, G. M. Koju, would like to acknowledge the financial assistance received from the TU Janasakti Bikash Tatha Kalyan Program, Coordination Division of the Rector's Office, Tribhuvan University, Nepal. The author is also grateful to the India Science and Research Fellowship (ISRF) Program for its assistance. Gratitude is also due to CSIR-Central Electrochemical Research Institute, Karaikudi, Tamil Nadu, India, for providing the laboratory facilities for conducting the present study.

DATA AVAILABILITY STATEMENT

The data presented in this study are available upon request from the corresponding authors.

CONFLICT OF INTEREST

The authors state that they have no conflicts of interests in this work.

REFERENCES

1. Callister W. D., Jr., Rethwisch D. G. (2018) Materials Science and Engineering: An introduction. Wiley, New York.

2. Watari T., Nansai K., & Nakajima K. (2021) Major Metals Demand, Supply, and Environmental Impacts to 2100: A Critical Review. *Resources, Conservation and Recycling,* **164**, 105107. https://doi.org/10.1016/j.resconrec.2020.105107

3. Alaneme K. K., Olusegun S. J., & Adelowo O. T. (2016) Corrosion Inhibition and Adsorption Mechanism Studies of Hunteria umbellata Seed Husk Extracts on Mild Steel Immersed in Acidic Solutions. *Alexandria Engineering Journal,* **55(1)**, 673–681. https://doi.org/10.1016/j.aej.2015.10.009

4. Rahal H., Abdel-Gaber A. M., El-Rifai M. S., & El-Housseiny S. (2024) The Potential of Natural Leaf Extracts as Green Inhibitors for Mild Steel Corrosion in Hydrochloric Acid Solutions. *Moroccan Journal of Chemistry,* **12(4)**, 1554–1574. https://doi.org/10.48317/IMIST.PRSM/MORJCHEM-V12I4.49691

5. Karki N., Neupane S., Gupta D. K., Das A. K., Singh S., Koju, G. M., Yadav, A. P. (2021) Berberine Isolated from Mahonia nepalensis as an Eco-friendly and Thermally Stable Corrosion Inhibitor for Mild Steel in Acid Medium. *Arabian Journal of Chemistry,* **14(12)**, 103423. https://doi.org/10.1016/j.arabjc.2021.103423

6. Ashassi-Sorkhabi H., Seifzadeh D., Hosseini M. G. (2008) EN, EIS and Polarization Studies to Evaluate the Inhibition Effect of 3H-phenothiazin-3-one, 7-dimethylamin on Mild Steel Corrosion in 1M HCl Solution. *Corrosion Science,* **50(12)**, 3363–3370. https://doi.org/10.1016/j.corsci.2008.09.022

7. Rahal H. T., Abdel-Gaber A. M., El Khatib L. W. (2023) Evaluation of Fragaria ananassa and Cucurbita pepo L Leaf Extracts as Natural Green Corrosion Inhibitors for Copper in 0.5 M Hydrochloric Acid Solution. *International Journal of Corrosion and Scale Inhibition,* **12(4)**. https://doi.org/10.17675/2305-6894-2023-12-4-4

8. Arthur D. E., Abechi S. E. (2019) Corrosion inhibition studies of mild steel using Acalypha chamaedrifolia leaves extract in hydrochloric acid medium. *SN Applied Sciences,* **1(9)**, 1089. https://doi.org/10.1007/s42452-019-1138-4

9. Al-Nami Samar. Y., Fouda A. E.-A. (2019) Calotropis Procera Extract as Corrosion Inhibitor for Copper in Nitric Acidic Environment. *International Journal of Electrochemical Science,* 6902–6919. https://doi.org/10.20964/2019.07.118

10. Chevalier M., Lebrini M., Robert F., Sutour S., Tomi F., Jama, C., Roos, C. (2019) Investigation of Corrosion Inhibition Efficiency of Amazonian Tree Alkaloids Extract for C38 Steel In 1M Hydrochloric Media. *International Journal of Electrochemical Science,* **14(2)**, 1208–1223. https://doi.org/10.20964/2019.02.38

11. Devikala S., Kamaraj P., Arthanareeswari M., Patel M. B. (2019) Green corrosion inhibition of mild steel by aqueous Allium sativum extract in 3.5% NaCl. *Materials Today: Proceedings,* **14**, 580–589. https://doi.org/10.1016/j.matpr.2019.04.182

12. Gupta D. K., Awasthi L., Das A. K., Yadav B., Ghimire A., & Yadav A. P. (2020) Corrosion Inhibition Effect of Acidic Extract of Bark of Eucalyptus Globulus on Mild Steel. *Tribhuvan University Journal,* **35(1)**, 1–10. https://doi.org/10.3126/tuj.v35i1.35828

13. Gupta D. K., Kafle K. A., Das A. K., Neupane S., Ghimire A., Yadav B. D., Yadav A. P. (2020) Study of Jatropha Curcas Extract as a Corrosion Inhibitor in Acidic Medium on Mild Steel by Weight Loss and Potentiodynamic Methods. *Journal of Nepal Chemical Society,* **41(1)**, 87–93. https://doi.org/10.3126/jncs.v41i1.30493

14. Chen S., Zhu B., Liang X. (2020) Corrosion Inhibition Performance of Coconut Leaf Extract as a Green Corrosion Inhibitor for X65 Steel in Hydrochloric Acid Solution. *International Journal of Electrochemical Science,* 1–15. https://doi.org/10.20964/2020.01.39

15. Karki N., Neupane S., Chaudhary Y., Gupta D. K., Yadav A. P. (2021) Equisetum hyemale: A New Candidate for Green Corrosion Inhibitor Family. *International Journal of Corrosion and Scale Inhibition,* **10(1)**, 206–227. https://doi.org/10.17675/2305-6894-2021-10-1-12

16. El-Housseiny S., Abdel-Gaber A. M., Rahal H. T., Beqai F. T. (2022) Eco-friendly Corrosion Inhibitor for Mild Steel in Acidic Media. *International Journal of Corrosion and Scale Inhibition.* https://doi.org/10.17675/2305-6894-2022-11-4-6

17. Karki N., Neupane S., Gupta D. K., Yadav A. P. (2023) Electrochemical Study on the Effect of Polar and Non-polar Extract of Artemisia vulgaris on the Corrosion Inhibition of Mild-Steel in an Acidic Medium. *RSC Advances,* **13(11)**, 7603–7613. https://doi.org/10.1039/D3RA00148B

18. Abomughaid M. M., Teibo J. O., Akinfe O. A., Adewolu A. M., Teibo T. K. A., Afifi M., Batiha G. E.-S. (2024) A phytochemical and pharmacological review of Ricinus communis L. *Discover Applied Sciences,* **6(6)**, 315. https://doi.org/10.1007/s42452-024-05964-5

19. Kumar M. (2017) A Review on Phytochemical Constituents and Pharmacological Activities of Ricinus communis L. Plant. *International Journal of Pharmacognosy and Phytochemical Research,* **9(4)**. https://doi.org/10.25258/phyto.v9i4.8116

20. Jena J., Gupta A. K. (2012) RICINUS COMMUNIS LINN: A PHYTOPHARMACOLOGICAL REVIEW, *International Journal of Pharmacy and Pharmaceutical Sciences* **4(4)**, 25-29.

21. Faustin M., Lebrini M., Robert F., Roos C. (2011) Corrosion Studies of C38 Steel by Alkaloids Extract of a Tropical Plant Type. *Int. J. Electrochem. Sci.,* **6**, 4095-4113. https://doi.org/10.1016/S1452-3981(23)18313-1

22. Koju G. M., Neupane S., Gupta D. K., Barik R. C., Karki N., Yadav A. P. (2026) Alkaloids from methanolic extract of Berberis asiatica as a potential corrosion inhibitor for active metal. *Results in Chemistry,* **20**, 102982. https://doi.org/10.1016/j.rechem.2025.102982

23. Pratiwi R. A., Nandiyanto A. B. D. (2022) How to Read and Interpret UV-VIS Spectrophotometric Results in Determining the Structure of Chemical Compounds. *Indonesian Journal of Educational Research and Technology,* **2(1)**, 1–20. https://doi.org/10.17509/ijert.v2i1.35171

24. Nandiyanto A. B. D., Oktiani R., Ragadhita R. (2019) How to Read and Interpret FTIR Spectroscope of Organic Material. *Indonesian Journal of Science and Technology,* **4(1)**, 97–118. https://doi.org/10.17509/ijost.v4i1.15806

25. Karki N., Neupane S., Chaudhary Y., Gupta D. K., Yadav A. P. (2020) Berberis Aristata: A Highly Efficient and Thermally Stable Green Corrosion Inhibitor for Mild Steel in Acidic Medium. *Analytical& Bioanalytical Electrochemistry,* **12(7)**, 970–988. http://www.abechem.com/article_43505.html

26. Patel N. S., Hadlicka J., Beranek P., Salghi R., Bouya H., Ismat H. A., Hammouti, B. (2014) Corrosion Inhibition of Steel by Various Parts of Rotula Aquatica Plant Extracts in H2SO4 Solutions: *Portugaliae Electrochimica Acta,* **32(6)**, 395–403. https://doi.org/10.4152/pea.201406395

27. Krishnaveni K., Ravichandran J. (2014) Effect of aqueous extract of leaves of Morinda tinctoria on corrosion inhibition of aluminium surface in HCl medium. *Transactions of Nonferrous Metals Society of China,* **24(8)**, 2704–2712. https://doi.org/10.1016/S1003-6326(14)63401-4

28. Murari, A., A, A., Sirimahachai, U., Rao, S., Hegde, G. (2026) Corrosion inhibition of mild steel using eco-friendly porous nanocarbon derived from waste mango kernels: a step towards sustainability. *RSC Advances,* **16(8)**, 6915–6930. https://doi.org/10.1039/D5RA09725H

29. Kairi N. I., Kassim J. (2013). The Effect of Temperature on the Corrosion Inhibition of Mild Steel in 1 M HCl Solution by Curcuma Longa Extract. *International Journal of Electrochemical Science,* **8(5)**, 7138–7155.

https://doi.org/10.1016/S1452-3981(23)14836-X

30. Pandey B., Pandey D., Pant N. P., Bhattarai D. P., Dhakal M., Oli, H. B. (2024) Methanol extract of Murraya koenigii stem as green inhibitor for mild steel corrosion in 1 M HCl solution. *Results in Surfaces and Interfaces,* **16**, 100245. https://doi.org/10.1016/j.rsurfi.2024.100245

31. Ostovari A., Hoseinieh S. M., Peikari M., Shadizadeh S. R., Hashemi S. J. (2009) Corrosion Inhibition of Mild Steel in 1M HCl Solution by Henna Extract: A Comparative Study of the Inhibition by Henna and Its Constituents (Lawsone, Gallic acid, α-d-Glucose and Tannic acid). *Corrosion Science,* **51**, 1935–1949. https://doi.org/10.1016/j.corsci.2009.05.024

32. Sadeghi Erami R., Amirnasr M., Meghdadi S., Talebian M., Farrokhpour H., Raeissi K. (2019) Carboxamide Derivatives as New Corrosion Inhibitors for Mild Steel Protection in Hydrochloric Acid Solution. *Corrosion Science,* **151**, 190–197. https://doi.org/10.1016/j.corsci.2019.02.019

33. Hamdy A., El-Gendy N. Sh. (2013) Thermodynamic, Adsorption and Electrochemical Studies for Corrosion Inhibition of Carbon Steel by Henna Extract in Acid Medium. *Egyptian Journal of Petroleum,* **22(1)**, 17–25. https://doi.org/10.1016/j.ejpe.2012.06.002

34. Odewunmi N. A., Umoren S. A., Gasem Z. M., Ganiyu Saheed. A., Muhammad Q. (2015) L-Citrulline: An Active Corrosion Inhibitor Component of Watermelon Rind Extract For Mild Steel In HCl Medium. *Journal of the Taiwan Institute of Chemical Engineers,* **51**, 177–185. https://doi.org/10.1016/j.jtice.2015.01.012

35. Salcı A., Yüksel H., Solmaz R. (2022) Experimental Studies on the Corrosion Inhibition Performance of 2-(2-Aminophenyl)Benzimidazole for Mild Steel Protection in HCl

Solution. *Journal of the Taiwan Institute of Chemical Engineers,* **134**, 104349. https://doi.org/10.1016/j.jtice.2022.104349

36. Bentiss F., Lebrini M., Lagrenée M. (2005) Thermodynamic Characterization of Metal Dissolution and Inhibitor Adsorption Processes In Mild Steel/2,5-Bis(N-Thienyl)-1,3,4-Thiadiazoles/Hydrochloric Acid System. *Corrosion Science,* **47(12)**, 2915–2931. https://doi.org/10.1016/j.corsci.2005.05.034

37. Mathina A., Rajalakshmi R. (2016) Corrosion Inhibition of Mild Steel in Acid Medium using Canna Indica as Green Corrosion Inhibitor. *RASAYAN J. Chem.*, **9(1)**, 56–66.

38. Kaya F., Solmaz, R., Geçibesler İ. H. (2023) Investigation of Adsorption, Corrosion Inhibition, Synergistic Inhibition Effect and Stability Studies of Rheum ribes Leaf Extract on Mild Steel in 1 M HCl Solution. *Journal of the Taiwan Institute of Chemical Engineers,* **143**, 104712. https://doi.org/10.1016/j.jtice.2023.104712

39. Zhao J., Zhao T., Zhang Y., Zhang Z., Chen Z., Wang J., & Chen M. (2024) Corrosion Behavior of the 2024 Aluminum Alloy in the Atmospheric Environment of the South China Sea Islands. *Coatings,* **14(3)**, 331. https://doi.org/10.3390/coatings14030331

40. Tan B., Zhang, S., He J., Li W., Qiang Y., Wang, Q., Chen, S. (2021) Insight into Anti-Corrosion Mechanism of Tetrazole Derivatives for X80 Steel in 0.5 M H2SO4 Medium: Combined Experimental and Theoretical Researches. *Journal of Molecular Liquids,* **321**, 114464. https://doi.org/10.1016/j.molliq.2020.114464

41. Alagta A., Felhösi I., Bertoti I., Kálmán E. (2008) Corrosion Protection Properties of Hydroxamic Acid Self-Assembled Monolayer on Carbon Steel. *Corrosion Science,* **50(6)**, 1644–1649. https://doi.org/10.1016/j.corsci.2008.02.008

42. Anadebe V. C., Chukwuike V. I., Chandra Nayak K., Ebenso E. E., Chandra Barik, R. (2024) Combined electrochemical, atomic scale-DFT and MD simulation of Nickel based metal organic framework (Ni-MOF) as corrosion inhibitor for X65 pipeline steel in CO2-saturated brine. *Materials Chemistry and Physics,* **312**, 128606. https://doi.org/10.1016/j.matchemphys.2023.128606

43. Chevalier M., Robert, F., Amusant N., Traisnel M., Roos, C., Lebrini M. (2014) Enhanced Corrosion Resistance of Mild Steel in 1M Hydrochloric Acid Solution by Alkaloids

Extract from Aniba rosaeodora Plant: Electrochemical, Phytochemical and XPS Studies. *Electrochimica Acta,* **131**, 96–105. https://doi.org/10.1016/j.electacta.2013.12.023

44. El Hamdani N., Fdil R., Tourabi M., Jama, C., Bentiss F. (2015) Alkaloids Extract of Retama monosperma (L.) Boiss. Seeds used as Novel Eco-friendly Inhibitor for Carbon Steel Corrosion in 1 M HCl Solution: Electrochemical and Surface Studies. *Applied Surface Science,* **357**, 1294–1305. https://doi.org/10.1016/j.apsusc.2015.09.159

45. Raja P. B., Qureshi A. K., Abdul Rahim A., Osman, H., Awang K. (2013) Neolamarckia cadamba Alkaloids as Eco-Friendly Corrosion Inhibitors for Mild Steel In 1M HCl Media. *Corrosion Science,* **69**, 292–301. https://doi.org/10.1016/j.corsci.2012.11.042